Journal of the Korean Physical Society, Vol. 50, No. 6, June 2007, pp. 1952∼1958

Polarized Effects in Optical Lithography with High NA Technology

Sang-Kon Kim*
School of Information, Communications and Electronics Engineering, Catholic University of Korea, Bucheon 420-743

(Received 5 September 2006, in final form 30 March 2007)

Since 193 nm is a practical wavelength, for the further improvement of the resolution, the high numerical aperture technologies of the 193 nm ArF lithography prolong and start its lithography ending. Application of polarization illumination leads to a 25 % increase in depth of focus and exposure latitude. Hence, polarization simulation becomes a key technology for its control and application. In this paper, the polarization of the numerical aperture is modeled into aerial images by using a vector model as an improved scalar model. In terms of small half pitch nodes, polarized effects are described in aerial and resist images. For high numerical aperture, the TM polarized degradation observed in the aerial and the resist images are severe, so a reduction of the TM polarization is required for below 45 nm half pitch pattern formation. In comparison with unpolarized small half pitch formation, the optical proximity effects of TE polarization are similar for dense patterns, but those effects are different for sparse patterns. Hence, the sparse pattern formation of TE polarization due to pitch size ratio is preferred to optical proximity correction.

PACS numbers: 85.40.Hp, 78.20.Bh, 85.40.Bh
Keywords: Lithography, Lithography simulation, Polarization, Numerical aperture, NA

I. INTRODUCTION

Since 193 nm is a practical wavelength, high numerical aperture (NA) technology of the ArF lithography is one of the remaining ways for further improvement of the resolution. For high NA systems, the vector nature of light cannot be neglected, and a vector diffraction theory is clearly needed to account for the inherent coupling between the vector components and the polarization of the electromagnetic field [1]. In an optical lithography imaging system, polarization can be distinguished into source polarization, mask polarization, and projection lens polarization such as lens pupil polarization. A lithography source produces source polarization. In a condenser lens, birefringence and polarization variation across the field are produced. In a mask, pattern induced polarization change, birefringence, and oblique incidence effects are produced. In a projection lens, polarization in the pupil plane, birefringence, and surface reflection are produced. In a wafer, the vector imaging effect and reflection at the resist surface are produced. Although wide and intensive simulation studies to apply vector and polarization models to lithography applications have been performed, the simple and effective algorithms of vector model are required for solving unexpected problems and for implementation of polarization technology. In this paper, the polarization effects of lithography illumination are described and modeled into aerial and resist images by using a vector model as an improvement over the scalar model.

II. POLARIZATION EFFECTS

The NA is defined as

$$NA = n \sin\theta \tag{1}$$

by using the sine of the approach angle (θ) of the ray and the refractive index (n) of material that the rays pass through. Under high NA, light travels at very large angles relative to the optical axis to come into interference at the imaging plane in terms of the Huygens-Fresnel principle. At large angles, the amount of constructive interference between two waves becomes highly dependent on the direction of the field vectors.

A plane wave is decomposed into a transverse electric (TE or s-polarized) field (Figure 1(a)) and a transverse magnetic (TM or p-polarized) field (Figure 1(b)) as it propagates from the entrance pupil to the exit pupil, all the way into the wafer plane [2, 3]. The Poynting vector is defined as the amount of energy that crosses, per unit time, an element of unit area perpendicular to the direction of propagation. The light intensity is assumed to be the absolute value of the time-averaged of Poynting vector which lies in the propagation direction.

$$I = |\langle \vec{S} \rangle| = |\langle \vec{E} \times \vec{H} \rangle|, \tag{2}$$

*Corresponding Author: sangkona@hotmail.com

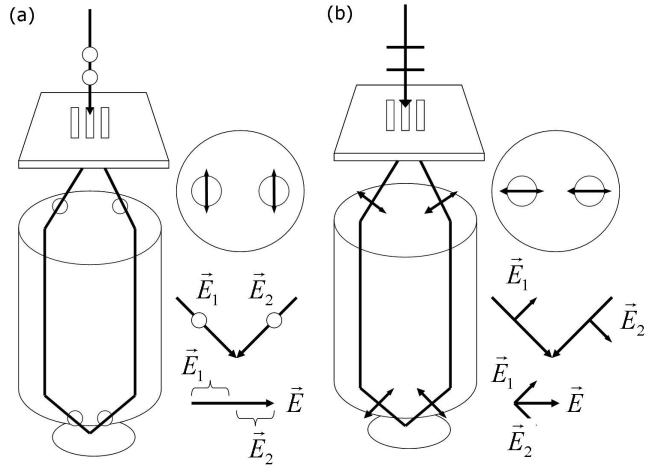

Fig. 1. Polarization representation of (a) the transverse electric (TE or s-polarized) field and (b) the transverse magnetic (TM or p-polarized) field.

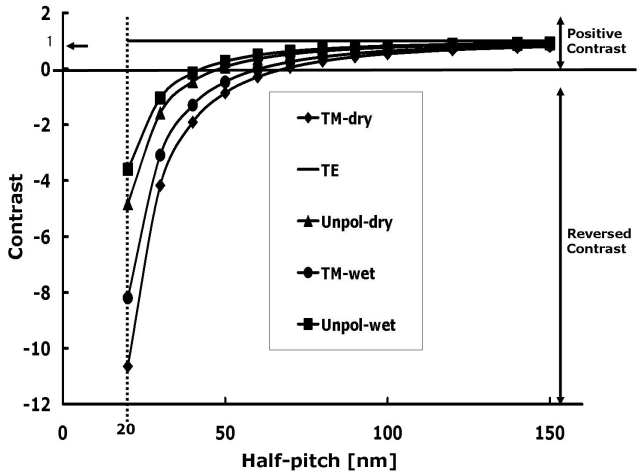

Fig. 2. Contrast degradations of TM and TM polarizations in dry and wet resists due to half-pitch sizes.

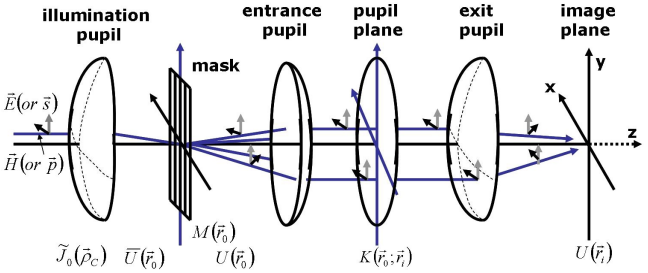

Fig. 3. Optical lithography imaging plane for scalar and vector models.

where $\vec{E}$ is the electric field and $\vec{H}$ is the magnetic filed. In a homogenous medium, the relation of the magnitudes of electromagnetic fields is $|\vec{E}| = \sqrt{\mu_m/\varepsilon_e}|\vec{H}|$, so that the intensity of light can be the square of the magnitude of the electric field (or the magnetic field). In the TE polarization of Figure 1(a), the electric fields of two plane waves overlap and interfere completely regardless of the angle between the plane waves. In the case of TE polarization, the total intensity of the waves for completed interfere is given by

$$I_{TE} = |\vec{E}_1 + \vec{E}_2|^2 = |\vec{E}_1|^2 + |\vec{E}_2|^2 + 2|\vec{E}_1|\vec{E}_2|. \qquad (3)$$

If the angle between the two plane waves is 2θ in the TM polarization of Figure 1(b), the geometric projection of the electric field vector E_2 in the same direction as E_1 is $E_2\cos(2\theta)$. The TM intensity is given by the coherent sum of the parts that overlap plus the incoherent sum of the parts that don't overlap:

$$\begin{aligned} I_{TM} &= |\vec{E}_1 + \vec{E}_2\cos(2\theta)|^2 + |\vec{E}_2\sin(2\theta)|^2 \\ &= |\vec{E}_1|^2 + |\vec{E}_2|^2 + 2|\vec{E}_1||\vec{E}_2\cos(2\theta)|. \end{aligned} \qquad (4)$$

If the permeability (μ_m) in the medium is equal to the permittivity (ε_e) in the medium and $|\vec{E}_1| = |\vec{E}_2| = 1$, the contrasts [$= (I_{max} - I_{min})/(I_{max} + I_{min})$] of the TE and the TM polarizations are 1 and $\cos(2\theta)$ by using Eqs. (3) and (4), respectively. These results mean not image contrast but a polarization effect on the contrast of the aerial image because the image contrast is a function of optical lithography parameters such as the illumination condition and the pattern in the mask [4, 5]. By using the Rayleigh equation ($HP = k_1 \times \lambda/NA$) and Eq. (1), the contrast of the TM polarization is

$$\begin{aligned} TMcontrast &= \cos(2\theta) = 1 - 2\sin^2\theta \\ &= 1 - 2\left[\frac{k_1\lambda}{n \cdot HP}\right]^2, \end{aligned} \qquad (5)$$

where k_1 is the process constant, λ is the wavelength, n is the refractive index, and HP is the half pitch.

Figure 2 shows the contrast degradations of the TM and the TE polarizations when k_1 is 0.25. Since the pattern size is smaller, the TM polarization effect on the contrast of the aerial image is more severe, and the contrast of the aerial image in water (n = 1.35) is better than that in air (n = 1). Hence, as NA increases, the imaging contrast is lower than the value obtained by using scalar imaging model due to the direction difference of the electric vectors of the interference light. The TE polarization (or s-polarized) illumination was proposed to increase the contrast of a high NA image [6].

III. SCALAR CALCULATION

For the optical lithography, the exposure system implements the *Köhler's* method, in which the illumination configuration forms an image of the light source onto the projection lens, thereby ensuring the absence of vignetting.

Figure 3 shows a representation of an optical lithography imaging plane for the scalar and the vector models. A quasi-monochromatic light source of a mean wave-

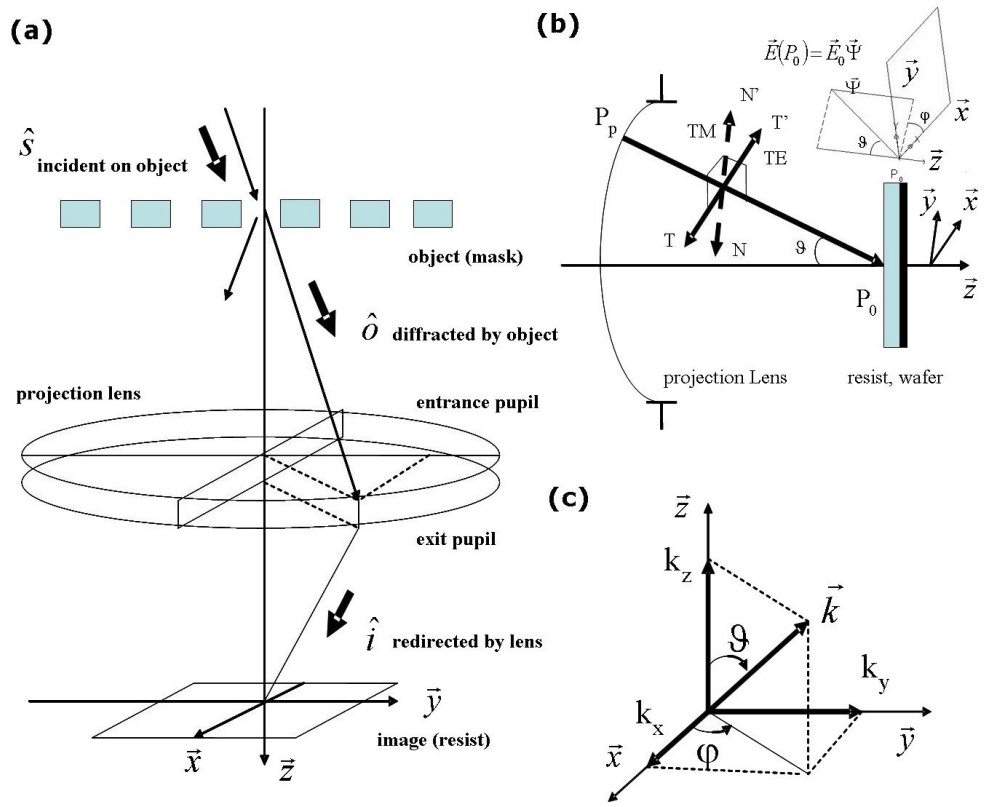

Fig. 4. (a) Schematic diagram of the wave vectors $\vec{s}$, $\vec{o}$, and $\vec{i}$ from the source, the mask, and the projection lens, respectively, (b) Ray $\vec{P_S P_0}$ through projection lens and (c) the direction cosines of a ray vector.

length illuminates the mask via the condenser lens. In conjunction with the condenser lens, the projection lens forms an image of the source on the pupil. The intensity on the wafer can be described by

$$
\begin{aligned}
I_i(\vec{r}_i) &= \langle U_i(\vec{r}_i;t)\, U_i^*(\vec{r}_i;t)\rangle \\
&= \iint_\Omega \langle U_0(\vec{r}_0;t)\, U_0(\vec{r}_0';t)\rangle \\
&\times K(\vec{r}_i-\vec{r}_0)\, K^*(\vec{r}_i-\vec{r}_0')\, d^2\vec{r}_0 d^2\vec{r}_0' \\
&= \iint_\Omega \left\langle \bar{U}_0(\vec{r}_0;t)\, \bar{U}_0(\vec{r}_0';t)\right\rangle M(\vec{r}_0)\, M^*(\vec{r}_0') \\
&\times K(\vec{r}_i-\vec{r}_0)\, K^*(\vec{r}_i-\vec{r}_0')\, d^2\vec{r}_0 d^2\vec{r}_0' \\
&= \iint_\Omega \bar{J}_0(\vec{r}_0-\vec{r}_0')\, M(\vec{r}_0)\, M^*(\vec{r}_0') \\
&\times K(\vec{r}_i-\vec{r}_0)\, K^*(\vec{r}_i-\vec{r}_0')\, d^2\vec{r}_0 d^2\vec{r}_0' \\
&= \iint \left[\int \widetilde{J}_0(\vec{\rho}_C)\, e^{-2\pi i\left(\vec{r}_i-\vec{r}_0'\right)\cdot\vec{\rho}_C} d^2\vec{\rho}_C\right] \\
&\times \left[\int \widetilde{M}(\vec{\rho}_P)\, e^{-2\pi i\vec{\rho}_P\cdot\vec{r}_0} d^2\vec{\rho}_P\right] \\
&\times \left[\int \widetilde{M}^*(\vec{\rho}_P')\, e^{-2\pi i\vec{\rho}_P'\cdot\vec{r}_0} d^2\vec{\rho}_P\right] \\
&\times K(\vec{r}_i-\vec{r}_0)\, K^*(\vec{r}_i-\vec{r}_0')\, d^2\vec{r}_0 d^2\vec{r}_0' \\
&= \iint \left[\iiint \widetilde{J}_0(\vec{\rho}_C)\, e^{-2\pi i\left(\vec{r}_i-\vec{r}_0'\right)\cdot\vec{\rho}_C}\right. \\
&\times K(\vec{r}_i-\vec{r}_0)\, K^*(\vec{r}_i-\vec{r}_0')\, e^{2\pi i\vec{\rho}_P\cdot(\vec{r}_i-\vec{r}_0)} \\
&\left.\times e^{-2\pi i\vec{\rho}_P'\cdot\left(\vec{r}_i-\vec{r}_0'\right)} d^2\vec{r}_0 d^2\vec{r}_0' d^2\vec{\rho}_C\right] \qquad (6) \\
&\times \widetilde{M}(\vec{\rho}_P)\, \widetilde{M}^*(\vec{\rho}_P')\, e^{-2\pi i\vec{\rho}_P\cdot\vec{r}_i} e^{-2\pi i\vec{\rho}_P'\cdot\vec{r}_0'} d^2\vec{\rho}_P d^2\vec{\rho}_P',
\end{aligned}
$$

where $U_i(\vec{r}_i;t)$ is the illumination distribution on the wafer, Ω is the integral area, $J(\vec{r}_i)$ is the mutual intensity, $M(\vec{r}_0)$ is the mask function, and $K(\vec{r}_i)$ is the transfer function of the projection lens [7,8]. Hence, the intensity on the wafer is

$$
\begin{aligned}
I(\vec{r}_i) &= \iint TCC(\vec{\rho}_P;\vec{\rho}_P')\, \widetilde{M}(\vec{\rho}_P)\, \widetilde{M}^*(\vec{\rho}_P') \\
&\times e^{-2\pi i\left(\vec{\rho}_P-\vec{\rho}_P'\right)\cdot\vec{r}_i} d^2\vec{\rho}_P d^2\vec{\rho}_P', \qquad (7) \\
TCC &= \iiint \widetilde{J}_0(\vec{\rho}_C)\bullet\widetilde{K}(\vec{\rho}_C+\vec{\rho}_P) \\
&\bullet\widetilde{K}^*(\vec{\rho}_C+\vec{\rho}_P')\, d^2\vec{\rho}_C, \qquad (8)
\end{aligned}
$$

where TCC is the transmission cross coefficients.

IV. VECTOR CALCULATION

In an optical lithography imaging system of high NA, three polarizations, source polarization, mask polarization, and lens pupil polarization, can be modeled for polarization effects.

Figure 4(a) shows a schematic diagram of the wave vectors. In the meridional plane, the wave vectors $\vec{s}$, $\vec{o}$, and $\vec{i}$ can be described as the direction vectors from the source, the mask, and the projection lens, respectively. The source vector $\vec{s}$ transforms into the object vector $\vec{o}$ through the mask, and the objective vector $\vec{o}$ transforms into the image vector $\vec{i}$ through the projection lens. It is an easy method to calculate the polarizations by using not those three vectors but one of those vectors. For the pattern induced polarization change in a mask, a vector model can be

$$I(\vec{r}_i) = \iint TCC(\vec{\rho}_P;\vec{\rho}'_P) \left[\sum_{\substack{i=\{x,y\}\\ j=\{x,y\}\\ k=\{x,y,z\}}} M_{0_{ik}}(\vec{\rho}_P) M^*_{0_{ik}}(\vec{\rho}'_P) E_j E^*_j \right] \widetilde{M}(\vec{\rho}_P) \widetilde{M}^*(\vec{\rho}'_P) e^{\left(\frac{2\pi}{\lambda}\right) i(\vec{\rho}_P - \vec{\rho}'_P)\cdot\vec{r}_i} d^2\vec{\rho}_P d^2\vec{\rho}'_P. \quad (9)$$

The extension from scalar partially coherent imaging to vector imaging involves replacing the scalar function $\widetilde{M}(\vec{\rho}_P)$ in Eq. (7) by the vector entity $\widetilde{M}(\vec{\rho}_P)$ $M_0(\vec{\rho}_P) E_0$. The vibrational direction of the electric field vector represents $M_0(\vec{\rho}_P) E_0$ [9]. For polarization in the pupil plane, a vector model can be

$$I(\vec{r}_i) = \sum_{k=x,y,z} \iint TCC_k(\vec{\rho}_P;\vec{\rho}'_P) \widetilde{M}(\vec{\rho}_P) \widetilde{M}^*(\vec{\rho}'_P) \times e^{\left(-\frac{2\pi}{\lambda}\right) i(\vec{\rho}_P - \vec{\rho}'_P)\cdot\vec{r}_i} d^2\vec{\rho}_P d^2\vec{\rho}'_P, \quad (10)$$

$$TCC_k(\vec{\rho}_P;\vec{\rho}'_P) = \int \widetilde{J}_0(\vec{\rho}_C) \bullet \widetilde{K}_k(\vec{\rho}_C + \vec{\rho}_P) \bullet \widetilde{K}^*_k(\vec{\rho}_C + \vec{\rho}'_P) d^2\vec{\rho}_C, \quad (11)$$

where $\vec{\rho}_P (= (f,g))$ is a normalized spatial frequency divided by NA/λ. The Fourier transform of the pupil function is

$$\widetilde{K}_k(\vec{\rho}_P) = \begin{cases} C\Psi_k(\widetilde{\rho}_P) e^{-\frac{2\pi}{\lambda} W(\vec{\rho}_P)}, & |\vec{\rho}_P| \langle 1, \\ 0, & otherwise \end{cases} \quad (12)$$

where the constant C is $\sqrt{\{1-(1+M^2)|\lambda\vec{\rho}_P|^2+|\lambda\vec{\rho}_P|^4\}}$, M is the magnification, $W(\vec{\rho}_P)$ is the aberration function, and $\Psi_k(\vec{\rho}_P)$ is the polarization distribution function. Figure 4(b) shows a ray $\overrightarrow{P_s P_0}$ through the projection lens. The field at P_0 is the vector sum of contributions from point sources on P_s of the projection lens. In Figure 4(b), the electric vector is composed of the transverse electric (TE) (or the perpendicular component ($\overrightarrow{TT'}$)) and the transverse magnetic (TM) (or the parallel component ($\overrightarrow{NN'}$)). The contribution of an image-forming ray to the vector field at the image point is proportional to

$$\vec{E}(P_0) = \vec{E}_0 \vec{\Psi}, \quad (13)$$

where $\vec{E}_0$ is a matrix of the field at P_0 in Figure 4(b) and $\vec{\Psi}$ is a matrix of polarizations. The overall polarization state can be written

$$\vec{\Psi} = \cos\phi \vec{\Psi}_x + e^{j\varphi} \sin\phi \vec{\Psi}_y, \quad (14)$$

where the angle φ is the phase difference between the x and the y modes. The angles ϕ and φ determine the actual polarization state. In the case of oblique incident rays, the x- and the y-polarization vectors can be further decomposed in terms of two unit vectors that are either parallel (TM) or perpendicular (TE) to the meridional plane [2]. When the direction cosines of a ray vector represent its propagation direction, the direction cosines (α, β, γ) in Figure 4(c) can be assumed to be given by

$$\alpha = \sin\vartheta\cos\varphi,\ \beta = \sin\vartheta\sin\varphi,\ \gamma = \cos\vartheta. \quad (15)$$

When the corresponding wave vector is $\vec{k} = k(\alpha,\beta,\gamma)$, the perpendicular direction ($\hat{s}_\perp$) to the meridional plane can be defined to be

$$\vec{s}_\perp = \frac{\vec{k}\times\hat{z}}{\left|\vec{k}\times\hat{z}\right|} \rightarrow s_{\perp x} = \frac{\beta}{\sqrt{1-\gamma^2}},\ s_{\perp y} = -\frac{\alpha}{\sqrt{1-\gamma^2}},\ s_{\perp z} = 0. \quad (16)$$

The fraction ($\vec{\Psi}_{x\perp}$) of x-polarized light that aligns with the perpendicular direction is assumed as

$$\vec{\Psi}_{x\perp} = \hat{x} \bullet \hat{s}_\perp. \quad (17)$$

Hence, the TE-polarized distribution functions are

$$\vec{\Psi}_{x\perp x} = \vec{\Psi}_{x\perp}(\hat{s}_\perp \bullet \hat{x}) = \frac{\beta}{1-\gamma^2},$$

$$\vec{\Psi}_{y\perp x} = \vec{\Psi}_{y\perp}(\hat{s}_\perp \bullet \hat{x}) = -\frac{\alpha\beta}{1-\gamma^2},$$

$$\vec{\Psi}_{x\perp y} = \vec{\Psi}_{x\perp}(\hat{s}_\perp \bullet \hat{y}) = -\frac{\alpha\beta}{1-\gamma^2},$$

$$\vec{\Psi}_{y\perp y} = \vec{\Psi}_{y\perp}(\hat{s}_\perp \bullet \hat{y}) = \frac{\alpha^2}{1-\gamma^2},$$

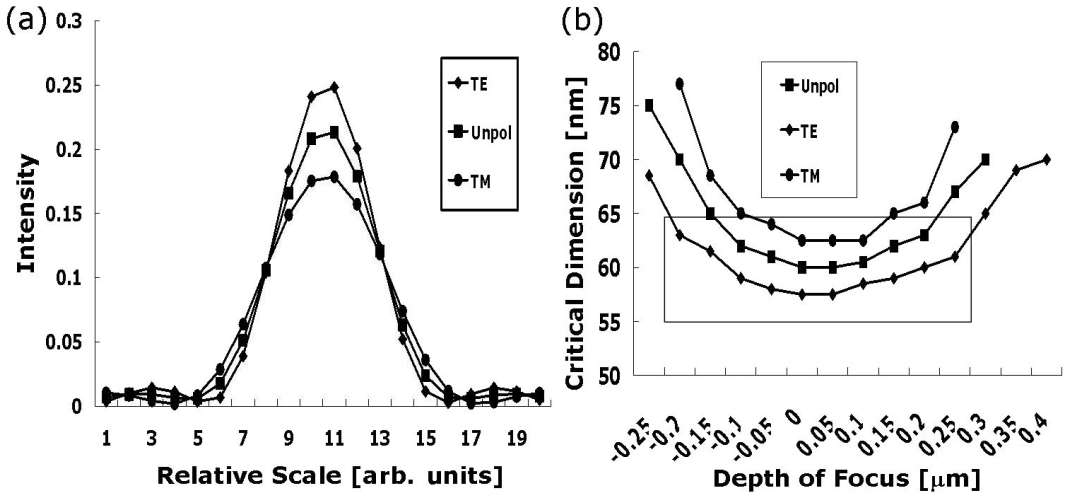

Fig. 5. Simulation results of (a) aerial images and (b) the process latitude of depth of focus (DOF) for polarization effects.

$$\vec{\Psi}_{x\perp z} = \vec{\Psi}_{x\perp}\left(\hat{s}_\perp \bullet \hat{z}\right) = 0,$$
$$\vec{\Psi}_{y\perp z} = \vec{\Psi}_{y\perp}\left(\hat{s}_\perp \bullet \hat{z}\right) = 0. \quad (18)$$

the TM component, the perpendicular direction ($\hat{s}_\parallel$) to the meridional plane can be defined as

$$\vec{s}_\parallel = \vec{k} \times \hat{s}_\perp \rightarrow\ s_{\parallel x} = \frac{\alpha\gamma}{\sqrt{1-\gamma^2}},$$
$$s_{\parallel y} = -\frac{\beta\gamma}{\sqrt{1-\gamma^2}},\ s_{\parallel z} = -\sqrt{1-\gamma^2}. \quad (19)$$

Following a development similar to the TM polarization, the TM-polarized distribution functions are

$$\vec{\Psi}_{x\parallel x} = \vec{\Psi}_{x\parallel}\left(\hat{s}_\parallel \bullet \hat{x}\right) = \frac{\alpha^2\gamma}{1-\gamma^2},$$
$$\vec{\Psi}_{y\parallel x} = \vec{\Psi}_{y\parallel}\left(\hat{s}_\parallel \bullet \hat{x}\right) = \frac{\alpha\beta\gamma}{1-\gamma^2},$$
$$\vec{\Psi}_{x\parallel y} = \vec{\Psi}_{x\parallel}\left(\hat{s}_\parallel \bullet \hat{y}\right) = \frac{\alpha\beta\gamma}{1-\gamma^2},$$
$$\vec{\Psi}_{y\parallel y} = \vec{\Psi}_{y\parallel}\left(\hat{s}_\parallel \bullet \hat{y}\right) = \frac{\beta^2\gamma}{1-\gamma^2},$$
$$\vec{\Psi}_{x\parallel z} = \vec{\Psi}_{x\parallel}\left(\hat{s}_\parallel \bullet \hat{z}\right) = -\alpha,$$
$$\vec{\Psi}_{y\parallel z} = \vec{\Psi}_{y\parallel}\left(\hat{s}_\parallel \bullet \hat{z}\right) = -\beta. \quad (20)$$

Summing the TE and the TM polarizations, the overall polarization states of Eq. (14) are

$$\vec{\Psi} = \begin{bmatrix} \vec{\Psi}_{x\perp x} + \vec{\Psi}_{x\parallel x} & \vec{\Psi}_{y\perp x} + \vec{\Psi}_{y\parallel x} \\ \vec{\Psi}_{x\perp y} + \vec{\Psi}_{x\parallel y} & \vec{\Psi}_{y\perp y} + \vec{\Psi}_{y\parallel y} \\ \vec{\Psi}_{x\parallel z} & \vec{\Psi}_{y\parallel z} \end{bmatrix} \quad (21)$$

The direction cosines of Eq. (15) are redefined by the normalized frequency variables:

$$\alpha = \hat{f}\sin\theta_{obj},\ \beta = \hat{g}\sin\theta_{obj},\ \gamma$$
$$= \sqrt{1-\left(\hat{f}^2+\hat{g}^2\right)\sin^2\theta_{obj}}. \quad (22)$$

To obtain the aerial image intensity of unpolarized light, the image intensities for TE and TM polarizations are calculated separately, and an average of those intensities is taken.

V. SIMULATION AND ANALYSIS

For the calculation of the scalar aerial image, we perform a Fourier transform of the rectangular mask according to the input parameters of the lens, such as the numerical aperture (NA), the partial coherence, the wavelength, and the defocus. The Fourier transform of mask pattern is added to those for the rectangular mask. The TCC is then calculated to get the common area among the pupil function, the conjugation of the pupil function, and the mutual intensity of the effective source. Hence, the scalar aerial image is obtained from the inverse Fourier transform of the multiplication results between the mask calculation and the TCC calculation [8]. For the calculation of vector aerial image, the pupil function is modified as the polarization pupil function in Eq. (8) in terms of the direction cosines as the normalized frequency variables.

Figure 5 shows the simulation results of aerial images and the process latitude of depth of focus (DOF) for polarization effects. The simulation conditions are a 193 nm wavelength, a 0.9 NA, a dipole (radius: 0.5, hole size: 0.3, angle: 45), a 6 % attenuated PSM for 60 nm line and space (L/S). In Figure 5(a), the intensity of the TE polarization is largest, so that the degradation of the intensity for the TM polarization is worst. Hence, the TE polarization has the best process latitude of DOF between the ±10 % range for the 60 nm pattern in Figure 5(b).

Figure 6 shows the simulated aerial and resist images of an acid and an inhibitor concentration due to the po-

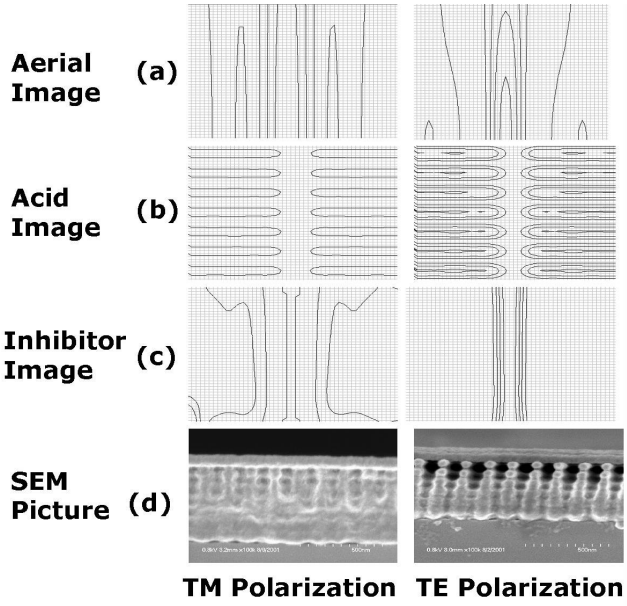

Fig. 6. Simulated bulk resist (a) aerial images, (b) acid after exposure and (c) the inhibitor concentration after post-exposure bake (PEB) for an isolated line, and (d) experimental SEM images for line and space patterns due to the TM and the TE polarization effects.

larization effects. Those resist bulk images are intensity distributions in Figure 6(a), the distributions of the acid concentration after exposure in Figure 6(b), the distributions of the inhibitor concentration after PEB in Figure 6(c) for a 50-nm pattern, and a SEM image of the 50-nm targeted L/S patterns in Figure 6(d) [10]. The images obtained by using TM polarization are so seriously degraded that those TM polarization images could not form patterns. Hence, TM and TE polarization form the different aerial and resist images.

Figure 7 shows the simulated optical proximity effects (OPEs) for TE polarization and for nopolarization, which is an average of the image intensities for TE and TM polarizations. When the pattern size is smaller and denser, the OPEs for both nopolarization and TE polarization are more severe to pattern formation, so an optical proximity correction (OPC) is required. When the pitch size is larger, the OPEs for nopolarization are constant in the pitch size ratio like those of a normal NA. However, the OPEs of TE polarization increase with increasing pitch size ratio. Hence, when polarization control is applied to optical lithography, due to pitch size ratio, the sparse pattern formation of TE polarization is preferred to the OPC. In terms of the pitch size ratio, the difference between the unpolarized critical dimension (CD) and the TE polarized CD can be assumed to be due to OPEs of polarization. An exponential function of the OPEs due to the pitch size ratio can be used in the model-based OPC [11,12].

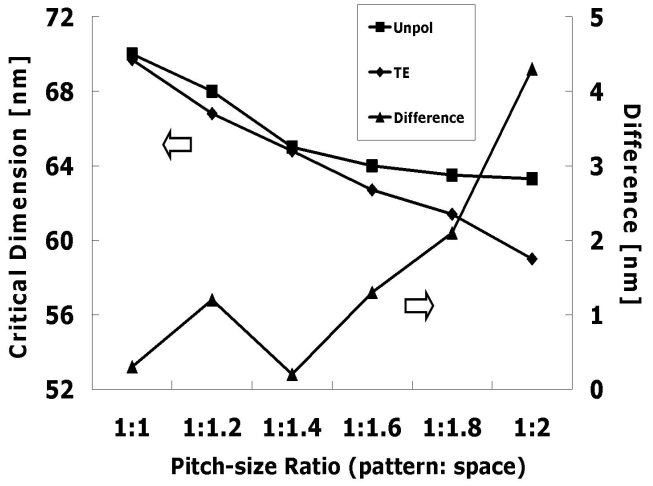

Fig. 7. Simulated optical proximity effects (OPCs) for nopolarization and TE polarization due to the pitch-size ratio.

VI. CONCLUSION

The polarization effects of a high NA are modeled into aerial and resist images by using a vector model as a simple improvement over the scalar model. For high NA, the TM polarized degradation of the aerial and the resist images are severe that a reduction of the TM polarization is required for below 45 nm half pitch pattern formation. In comparison with the unpolarized small half pitch formation, for dense and small pattern formation, the OPEs of both nopolarization and TE polarization are similar, so a similar OPC is required. However, for the sparse pattern formation, the OPEs of TE polarization increase with increasing pitch size ratio so that, due to pitch size ratio, TE polarization is preferred to OPC in the application of polarization control.

ACKNOWLEDGMENTS

This work was supported by the Korea Research Foundation Grant funded by the Korean Government (MOEHRD, Basic Research Promotion Fund) (KRF-2006-331-D00306).

REFERENCES

[1] B.-S Ahn, S. Y. Zinn, S.-W. Choi and J.-M. Sohn, Proc. SPIE **5040**, 1529 (2003).
[2] B. E. A. Saleh and M. C. Teich, *Fundamentals of Photonics* (John Wiley & Sons, New York, 1991), Chap. 6.
[3] M. McCallum, G. Fuller and S. Owa, Micro. Microelectron Eng. **83**, 667 (2006).
[4] J. R. Sheats and B. W. Smith, *Microlithography Science and Technology* (Marcel Dekker, New York, 1998), Chap. 3.

[5] P. Rai-Choudhury, *Microlithography, Micromaching and Microfabrication,* Vol. 1, *Microlithography* (SPIE, Washington, 1997), Chap. 1.
[6] M. Totzech, P. Graupner, T. Heil, A. Gohnermeier, O. Dittmann, D. Krahmer, V. Kamenov and J. Ruoff, Proc. SPIE **5754**, 23 (2005).
[7] J. B. Park, Ph.D. thesis, Seoul National University, 2002.
[8] S.-K. Kim and H.-K. Oh, J. Korean Phys. Soc. **41**, 456 (2002).
[9] A. K. Wong, *Optical Imaging in Projection Microlithography* (SPIE, New York, 2005), p. 106.
[10] M. I. Sanchez, F. A. Houle, J. A. Hoffnagle, T. A. Brunner and W. D. Hinsberg, Proc. SPIE **4690**, 351 (2002).
[11] S.-K. Kim and T. S. Kim, J. Korean Phys. Soc. **48**, 1661 (2006).
[12] S.-K. Kim and H.-K. Oh, J. Korean Phys. Soc. **47**, S377 (2005).